ORIGINAL ARTICLE

Directionality of Cavities and Porosity Formation in Powder-Bed Laser Additive Manufacturing of Metal Components Investigated Using X-Ray Tomography

Anton du Plessis,[1] Stephan Gerhard le Roux,[1] Gerrie Booysen,[2] and Johan Els[2]

Abstract

Ensuring additive manufactured metal components are free of major defects is crucial to the application of this new technology in medical and aerospace industries. One source of defects in such parts is lack of fusion in individual locations or specific layers. Such lack of melting or fusion could be the result of a nonflat powder bed due to an imperfect recoating blade or loose support structures causing recoating problems. Another possible source is laser power fluctuations or beam size fluctuations, or even ambient humidity or temperature changes, among others. The aims of this article are to investigate lack of fusion with planned induced defects (cavities) with different three-dimensional (3D) geometries and analyze these using nondestructive 3D X-ray tomography. It is found that some fusion occurs in induced defect layers and lines perpendicular to the build direction (XY) up to 180 μm in height. This means fusion occurs through fused layers above cavities, minimizing defect formation in the plane of the build platform. In contrast, in the case of vertical cavities (cavity walls) parallel to the build direction, much larger defects are observed compared to the above case. This result may point to the build direction (vertical) being more favorable for porosity formation under nonideal conditions (i.e., a preferred directionality). An example of unexpected porosity trail formation in the build direction is also reported from such nonideal conditions for a real part in contrast to a designed cavity.

Introduction

ADDITIVE MANUFACTURING OF metals is growing steadily with many applications[1] among others in the medical[2] and aerospace[3] industries. In these industries, in particular, it is extremely important to produce parts that are free of major defects (porosity). Various quality controls for the production of Ti6Al4V parts by this method are discussed in detail in the relevant ASTM standard.[4] The use of laboratory X-ray tomography to nondestructively detect defects in these parts makes it a unique tool for quality control and process optimization, with huge potential for 100% inspection. The X-ray tomography method has been reviewed for applications in materials sciences recently.[5] This method also has an ASTM standard, which ensures adequate quality of inspections, when adhering to some minimum requirements in scan parameters and analysis methods.[6] A recent review of nondestructive testing of additive manufactured components discusses various aspects, including the use of X-ray tomography.[7]

Various studies have been focused on the porosity of additive manufactured parts, and the levels of porosity can vary considerably depending on the system and the parameters used. Two main types of porosity are known to occur.[7] Lack of fusion defects are irregular shaped, and in contrast, gas entrapment porosity is very spherical. Generally, the average porosity in parts built to good specifications is >99.5% dense, that is, 0.5% porosity or less.

In an X-ray CT study of porosity of additive manufactured titanium parts, where the average porosity was reported in the range 0.1–0.5%, porosity trails were reported that followed the build direction.[8] Similar three-dimensional (3D) porosity images were reported at levels above 0.2% average porosity in other works.[2,9] In a very recent work, similar images are reported, and these results all indicate that the porosity structure may depend on the build direction.[10] All these examples show irregular porosity shapes indicating lack of fusion as the cause.

Some other examples of the use of X-ray tomography in studies of additive manufactured parts include a study of the

[1]CT Scanner Facility, Central Analytical Facilities, Stellenbosch University, Stellenbosch, South Africa.
[2]Centre for Rapid Prototyping and Manufacturing, Central University of Technology, Bloemfontein, South Africa.

porosity before and after HIP treatment at 22 μm resolution[11] and a study of 3D porosity and its relation to fatigue properties,[12] and the technique has also been used for process optimization for additive manufacturing of porous Ti6Al4V scaffold structures by full 3D analysis and optimization of the design in a second build cycle.[13] Some porosity analysis by CT analysis of additive manufactured metals is reported in the study by Becker *et al.*[14]

The authors of this present article have reported the methodology for nondestructive testing and qualification of additively manufactured medical implants at various resolutions and scan parameters (du Plessis et al., unpublished material). The general use of X-ray tomography in additive manufactured part inspection has also been reported in the study by du Plessis et al.[15] and recently has been shown to also be useful for dimensional accuracy assessment for consumer-grade 3D printing, where the same methodology can be applied to any additive process.[16]

Recently, a very flat layered form of defect was reported using X-ray tomography of an additive manufactured test part, which is speculated to be due to improper fusion in one or more layers of powder. This lack of fusion was speculated to be due to support structures of other parts in the build volume, which came loose and created lines across the powder bed in the recoating process, and these lines then caused improper fusion.[17]

In the present study, three test samples were made to investigate this lack of fusion phenomenon further. The aims are to create defect regions inside the parts with varying design sizes and analyze these defect regions in 3D using X-ray tomography. These defect regions were created by inserting cavities of known geometries into the CAD file and comparing the measured cavities from CT scans to the designed cavities.

Materials and Methods

Three test samples of titanium-6aluminum-4vanadium were manufactured on an EOS M280 using standard good quality build settings, as used in previous studies and as used routinely to build parts with less than 0.1% porosity on average. These settings include 170 W laser power, 1200 mm/s scanning speed, 100 μm spot size, and 30 μm layer thickness. The samples of $\sim$30 mm height and up to 20 mm width were produced with induced defect regions. These induced defects were fabricated by leaving cavities in the CAD file while keeping processing parameters exactly constant. One sample contains horizontal square layered defects in the XY plane, perpendicular to the build direction and with varying layer thicknesses, as shown in Figure 1. A second sample contains straight cylindrical tracks with different diameters, as shown
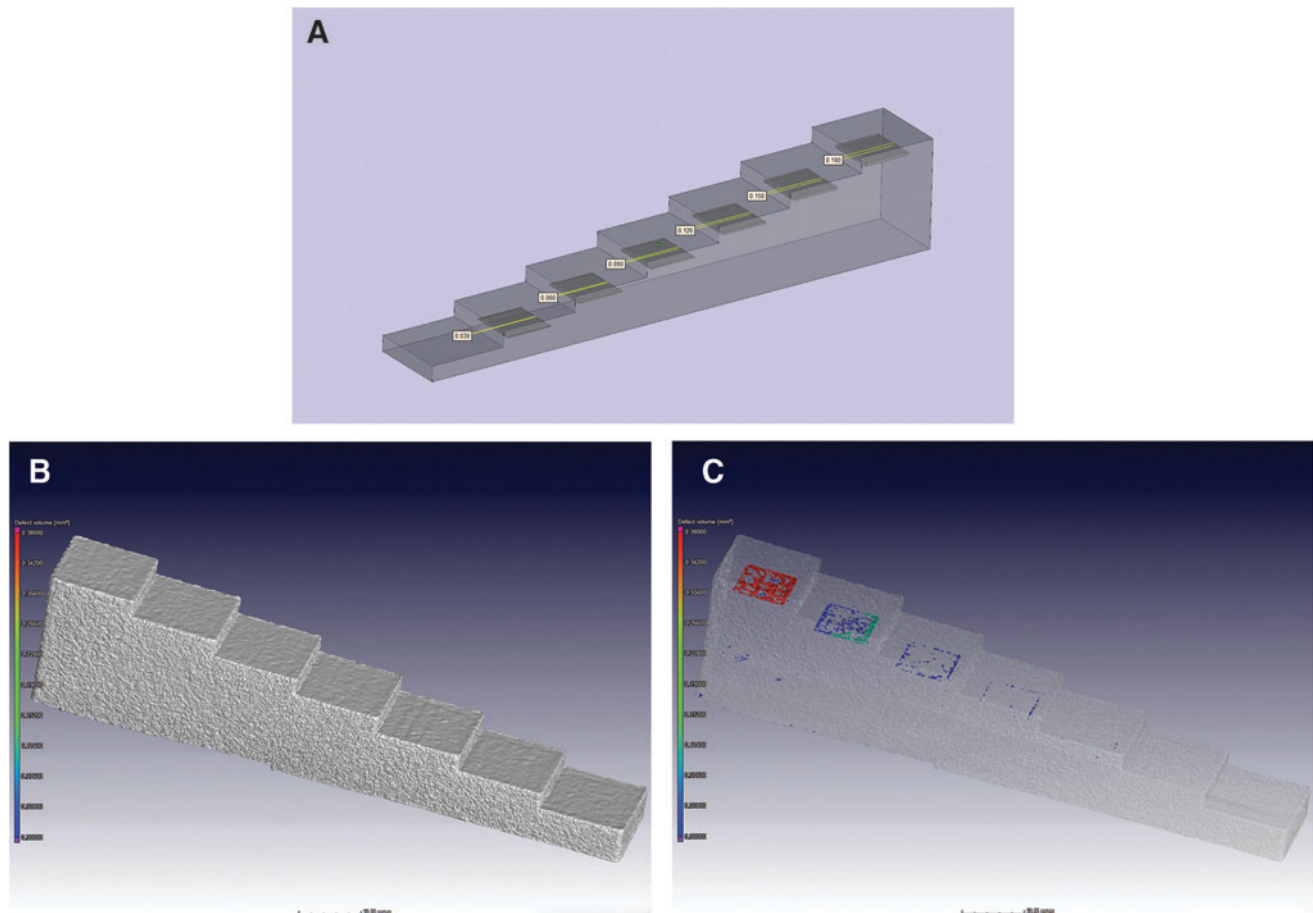

FIG. 1. The step sample with induced layered defects (*flat cavities*) of varying thicknesses perpendicular to the build direction: Shown here are the CAD file (**A**), the X-ray CT surface view (**B**), and a transparent CT defect analysis view (**C**). Color coding of defect volumes shows the largest defect in *red* and the smallest defect in *blue*. CT, computed tomography. Color images available online at www.liebertpub.com/3dp

in Figure 2. A third sample contains cubes with cube-shaped internal cavities with varying wall thicknesses, as shown in Figure 3.

A sample from another system with porosity trails is also reported from a laser cusing system under nonideal parameters. The system used was a Concept Laser Cusing M2 machine. This example is meant to show an extreme case of directionality of the porosity, which can be formed under nonideal build conditions.

The samples were subjected to X-ray micro-computed tomography (micro-CT) in the CT Scanner Facility at the Stellenbosch University. Micro-CT scans were done with a General Electric Phoenix V|Tome|X L240 system at voltages from 100 to 160 kV and 100–150 μA, 500 ms per image, with up to 3200 images in one full rotation. Image averaging and skipping are used to enhance image quality. Detector shift was activated to minimize rotation artifacts, and automatic scan optimization was activated. Reconstruction was done with system-supplied software, including beam hardening correction. All analyses reported here were done with Volume Graphics VGStudio Max 2.2, including the defect analysis

module. The software uses an advanced thresholding method, which allows subvoxel accuracy in the edge determination between material and void, and overcomes problems with slight variations in grayscale values across the images, which are typical of CT data. The subvoxel accuracy in surface determination is explained in more detail elsewhere.[18,19]

The micro-CT scans reported here were done at resolutions from 20 to 30 μm, such that the entire sample fits in a single-scan volume in each case. This results in detail detectability of at least the scan resolution, although automated defect analysis is done for pores larger than eight voxels only, which results in a minimum automated defect diameter of 60–90 μm in these scans, assuming a spherical pore geometry.

Results and Discussion

The designed step sample, which is shown in Figure 1, contains horizontal square defects with varying thicknesses from 180 to 30 μm. The X-ray CT results in Figure 1 show the surface of the sample, followed by a transparent view with an
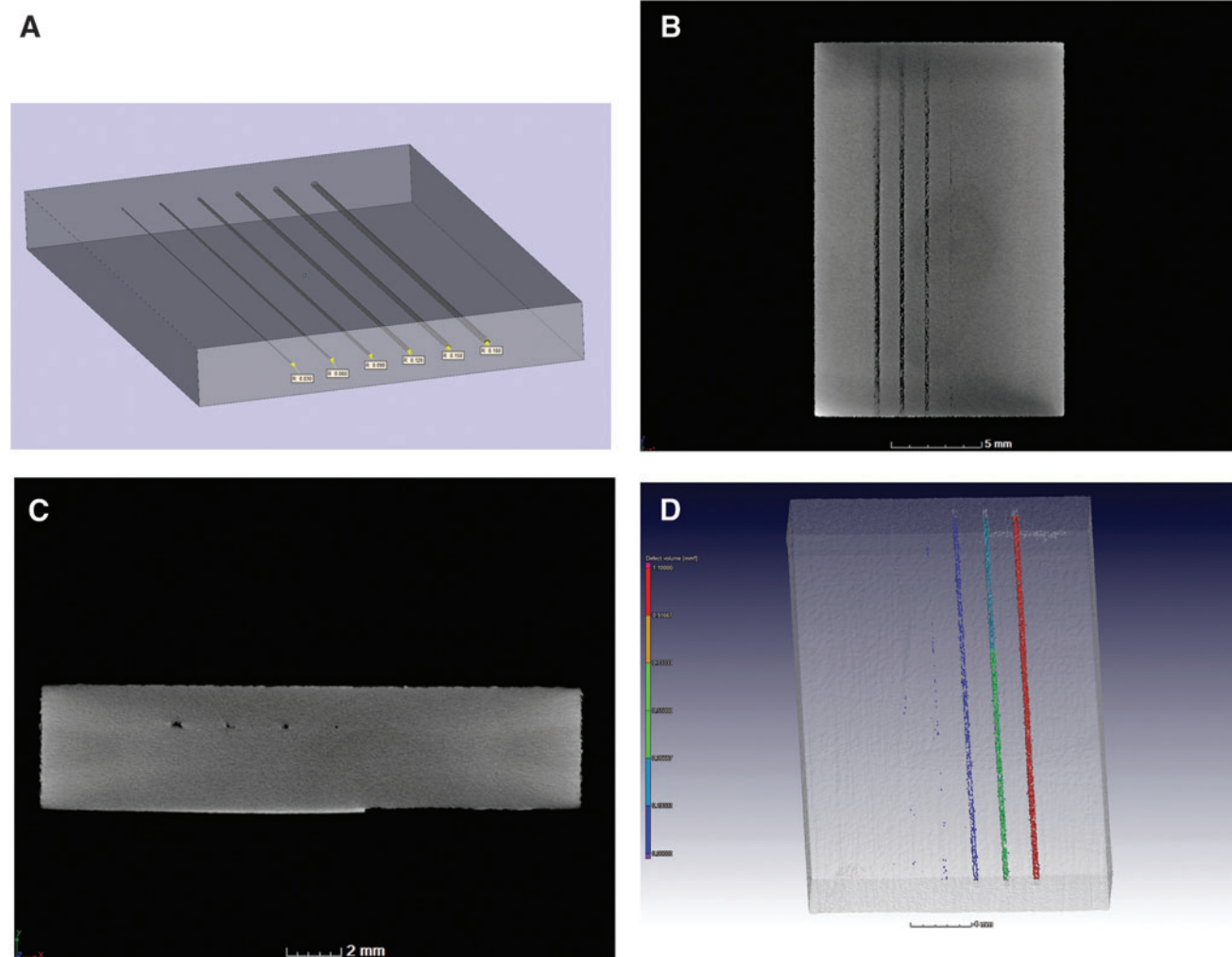

FIG. 2. The rectangular sample with induced line/track defects of varying thicknesses perpendicular to the build direction. Shown here are the CAD file (**A**), the X-ray CT slice images from *top* view (**B**) and *front* view (**C**), and a transparent CT defect analysis view (**D**). Color images available online at www.liebertpub.com/3dp
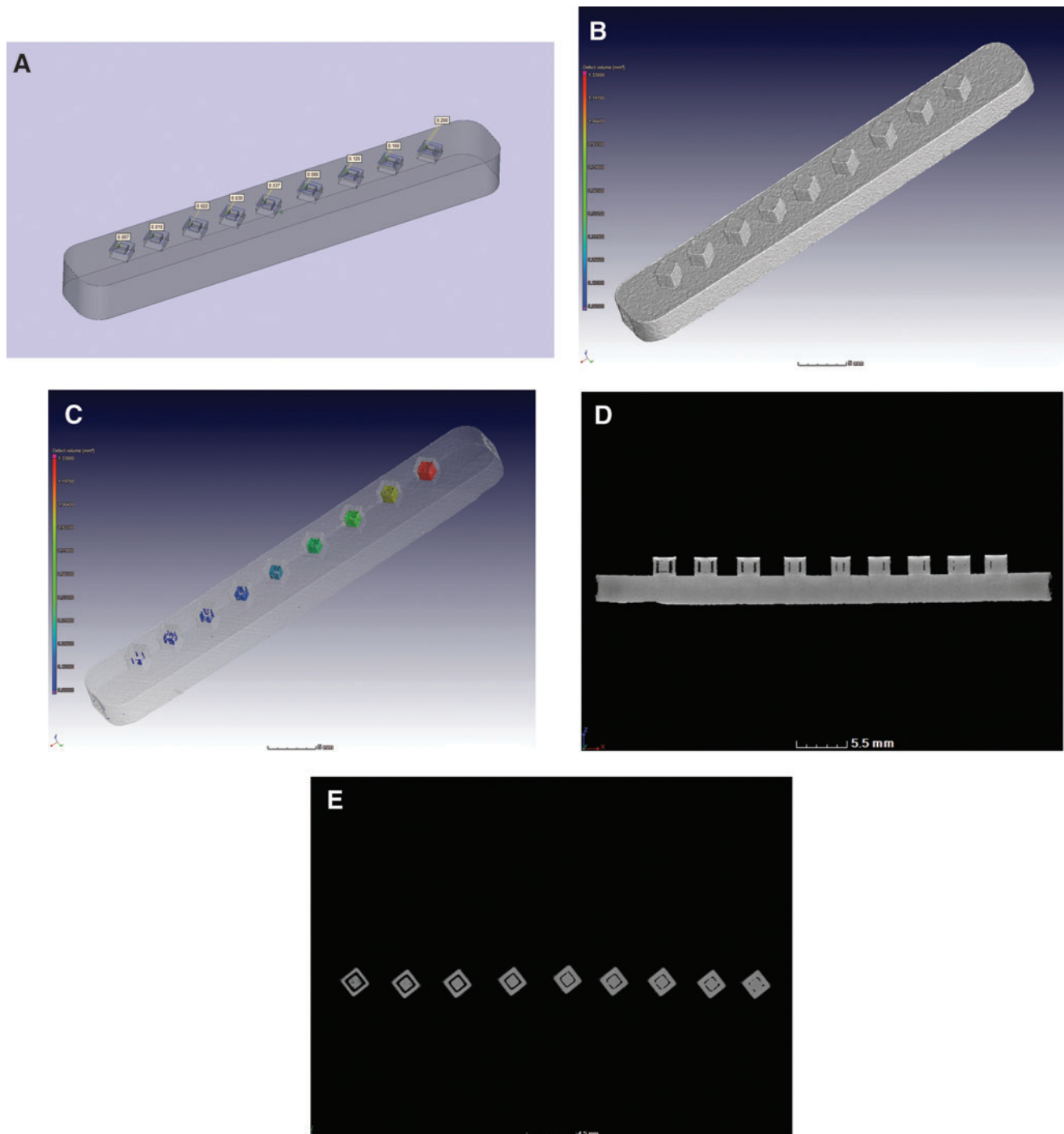
FIG. 3.   The cube sample with induced *vertical square* defects of varying thicknesses parallel to the build direction: Shown here are the CAD file (**A**), the X-ray CT surface view (**B**), a transparent CT defect analysis view (**C**), and CT slice images from *side* (**D**) and *top* (**E**) views. Color images available online at www.liebertpub.com/3dp

automated defect analysis showing a color-coded defect analysis, that is, red showing the largest pore by volume. In this way, it is clear that the first four defect layers are detected, that is, from 180 to 90 μm. It is also clear that the layer thickness varies and is not fully pore space, that is, it is partially solid. This is speculated to be due to remelting from subsequent layers, causing the internal regions to fuse together. Figure 4 shows the same results, but with slice images

in the plane of each successive layer, showing good contrast images of the porosity regions. In this case, it is clear that pores are also detected in the expected position of the 5th layer at 60 μm design thickness but no defects at the sixth and last layers with 30 μm design thickness. It is speculated that fusion occurs through the next layers above the cavity space during the build process, and it is quite surprising that this even occurs up to a cavity layer thickness of 180 μm.
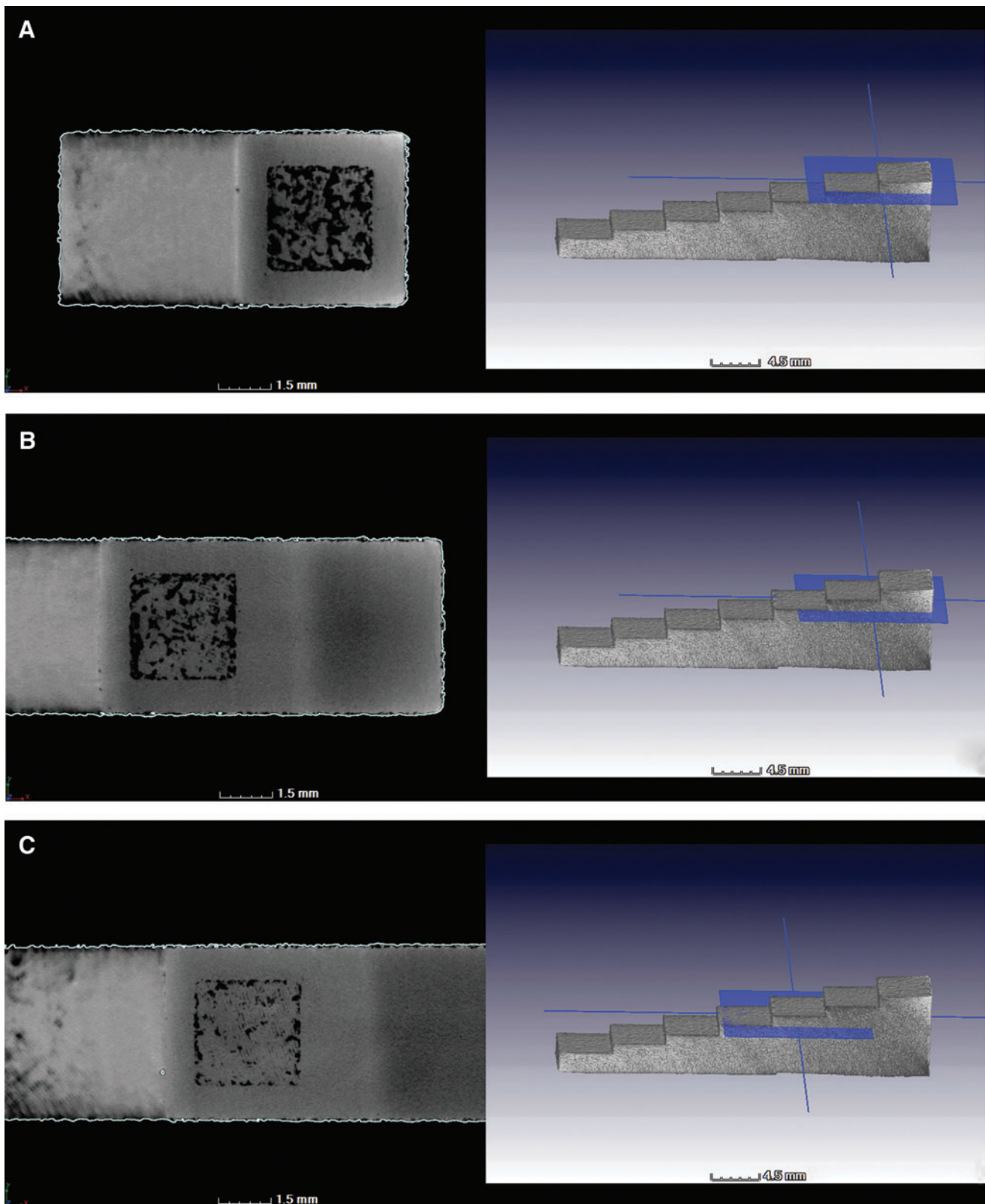
FIG. 4. CT slice images of each defect layer (induced cavity) in the plane of the layer showing good contrast images of the porosity for the steps from *top* to *bottom* in **(A–F)**. *Black* indicates void space, and *gray* areas indicate solid material. *Grayscale* variations are exaggerated as the defect areas are on the same height as the next step edge (the edge between material and air). Color images available online at www.liebertpub.com/3dp
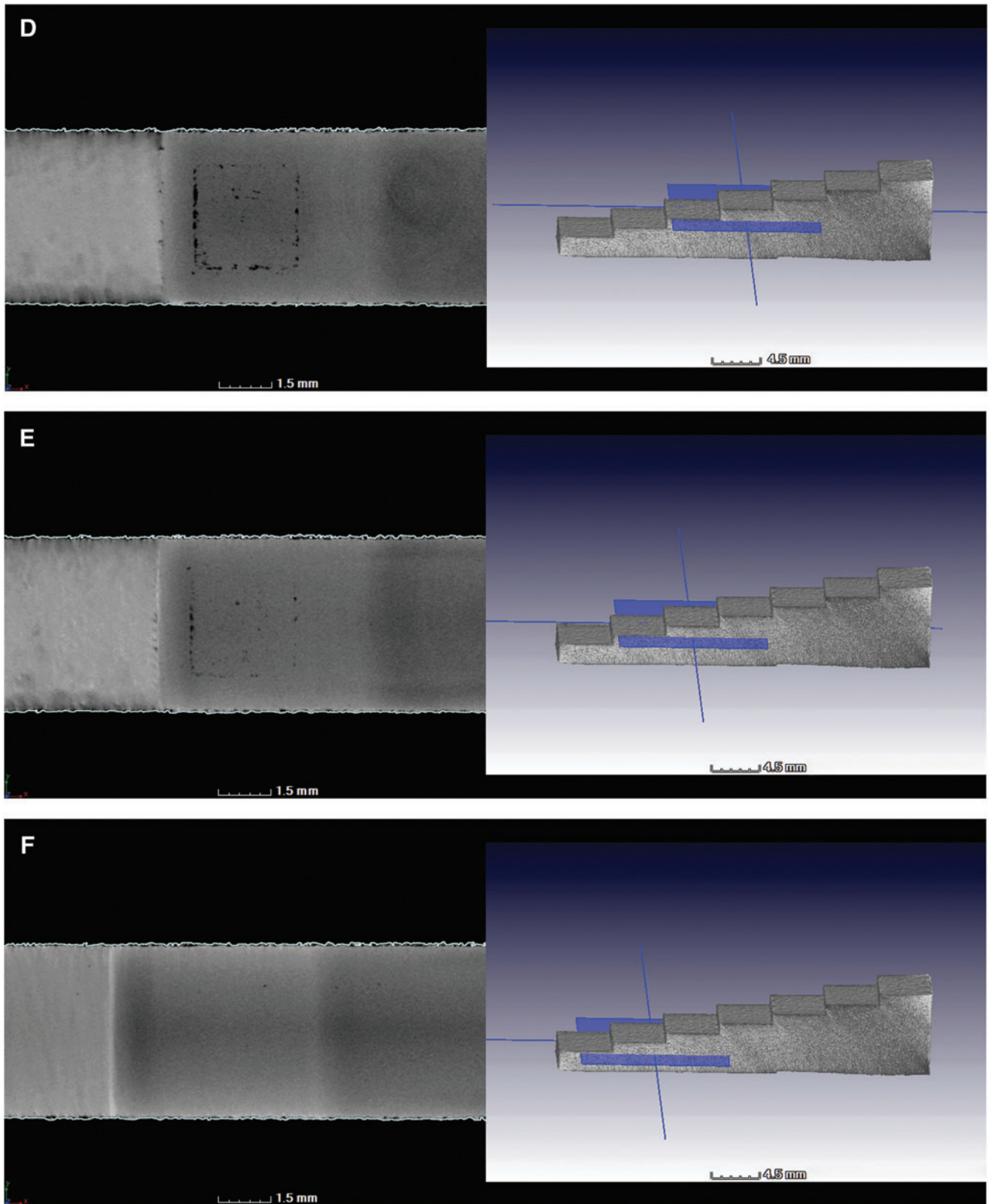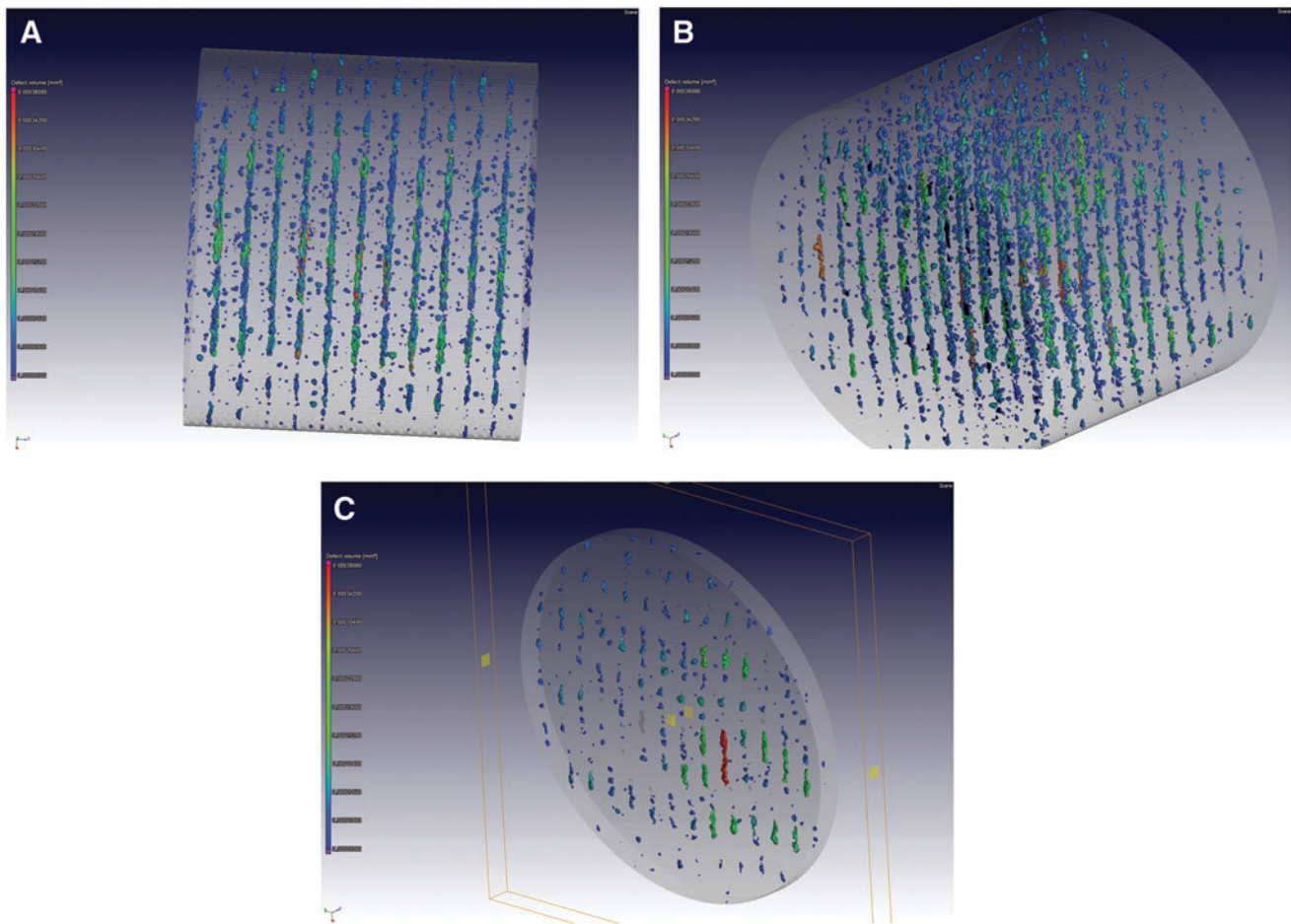
FIG. 4.   (Continued)

FIG. 5. Structured porosity found under nonideal build conditions on a different system, with porosity trails following the build direction. Shown here are CT defect analysis views from two directions **(A, B)** and one *cropped* view to emphasize the directionality of the porosity trails **(C)**. Color images available online at www.liebertpub.com/3dp

Figure 2 shows the test sample with defect lines/tracks at varying thicknesses and that such tracks are not fully pore space on their interior, similar to that seen in the previous example. In this case, the track of 90 μm diameter is only marginally detectable. The track of 60 μm is not seen, but some isolated pores are seen in the expected location of this track. The expected track of 30 μm is not seen at all. Again, it is speculated that these results are due to fusion of the layers above the cavity space, with similar results to those of the first test object.

In Figure 3, the test sample with cube-shaped defects is shown. The build direction is upward in the images, from the horizontal base still attached to the cubes. Therefore, the indicated cube-shaped defects have vertical cavity walls of varying thicknesses, parallel to the build direction. Clearly, all the defects are seen in the CT data, even the smallest designed 7 μm cavity wall thickness is seen clearly. The detected cavity walls of the designed 7 μm width are in fact 70 μm wide in places (as measured by CT), making this type of induced defect much larger than expected.

In the first two examples, it was shown that fusion occurs through subsequent layers, melting above cavities in the XY plane, causing those cavities to be thinner than expected. However, for cavities in the Z direction, no such fusion occurs. The height of these vertical cavities is as expected, and the width of these features is found to be larger than expected. This result indicates that any form of porosity might have a preferred directionality. Defects in the XY plane are minimized due to fusion through subsequent layers, while vertical Z-plane defects are not minimized in the same way.

In addition to the test specimens reported with induced defects, one example is shown in Figure 5 of unexpected porosity formation at levels of 0.6% average porosity. The sample was built on a different system with nonideal parameters, the details of which will not be reported here as it is still under investigation. It is relevant to report this example since the porosity is well structured in a checkerboard pattern but tends to produce trails in one direction, specifically in the build direction. This observation seems to validate the above discussion with regard to porosity preferentially forming in the build direction. In this case, the demonstration is for unexpected porosity rather than only induced defects as in the above three test samples. It is important to note that the observation of directionality is not limited to one type of defect and would most likely occur with any type of internal cavity or defect and will therefore affect the design of parts with internal cavities.

Conclusions

Defects were designed and induced in the additive manufacturing of test samples of titanium, with different defect design geometries. The results indicate that defects up to $180\,\mu m$ in height significantly fuse together in subsequent layers, but vertical defects are found to be larger than expected, possibly due to the inverse effect: lack of fusion due to the large vertical shape of the defect. This indicates that vertical defects following the build direction can be preferentially formed and may be a general result for all types of defects and internal cavities in such parts. An example was also shown, where unexpected porosity (not designed cavity) follows the build direction, in a different system at higher levels of porosity.

The directionality of defects observed may be helpful to interpret quality issues of additive manufacturing of metal components and help designers or engineers to wisely select the building orientation when producing complex parts using selective laser melting methods.

This work may also be valuable to other researchers using X-ray tomography to investigate defects in additive manufactured parts and may act as a good reference. For this purpose, the design files are included as Supplementary Figures SF1–SF3 (Supplementary Data are available online at www.liebertpub.com/3dp).

Author Disclosure Statement

No competing financial interests exist.

References

1. Gu DD, Meiners W, Wissenbach K, Poprawe R. Laser additive manufacturing of metallic components: materials, processes and mechanisms. Int Mater Rev 2012;57:133–164.
2. Vandenbroucke B, Kruth JP. Selective laser melting of biocompatible metals for rapid manufacturing of medical parts. Rapid Prototyping J 2007;13:196–203.
3. Lyons B. Additive manufacturing in aerospace: examples and research outlook. Bridge 2014;44:13–19.
4. ASTM F2924-14. Standard Specification for Additive Manufacturing Titanium-6 Aluminum-4 Vanadium with Powder Bed Fusion. ASTM International, West Conshohocken, PA, 2014.
5. Maire E, Withers PJ. Quantitative X-ray tomography. Int Mater Rev 2014;59:1–43.
6. ASTM E1570-11. Standard Practice for Computed Tomographic (CT) Examination, ASTM International, West Conshohocken, PA, 2011.
7. Sharratt BM. Non-Destructive Techniques and Technologies for Qualification of Additive Manufactured Parts and Processes, Victoria, BC, 2015.
8. Léonard F, Tammas-Williams S, Prangnell PB, Todd I, Withers PJ. Assessment by X-ray CT of the effects of geometry and build direction on defects in titanium ALM parts. In Conference on Industrial Computed Tomography (ICT), 2012; pp. 19–21.
9. Kruth J-P, Levy G, Klocke F, Childs THC. Consolidation phenomena in laser and powder-bed based layered manufacturing. Ann CIRP 2007;56:730–759.
10. Ziółkowski G, Chlebus E, Szymczyk P, Kurzac J. Application of X-ray CT method for discontinuity and porosity detection in 316L stainless steel parts produced with SLM technology. Arch Civil Mech Eng 2014;14:608–614.
11. Leuders S, Thöne M, Riemer A, Niendorf T, Tröster T, Richard HA, et al. On the mechanical behaviour of titanium alloy TiAl6V4 manufactured by selective laser melting: fatigue resistance and crack growth performance. Int J Fatigue 2013;48:300–307.
12. Siddique S, Imran M, Rauer M, Kaloudis M, Wycisk E, Emmelmann C, et al. Computed tomography for characterization of fatigue performance of selective laser melted parts. Mater Design 2015;83:661–669.
13. Van Bael S, Kerckhofs G, Moesen M, Pyka G, Schrooten J, Kruth JP. Micro-CT-based improvement of geometrical and mechanical controllability of selective laser melted Ti6Al4V porous structures. Mater Sci Eng A 2011;528: 7423–7431.
14. Becker TH, Beck M, Scheffer C. Microstructure and mechanical properties of direct metal laser sintered Ti-6Al-4V. South Afr J Indus Eng [S.l.] 2015;26:1–10.
15. du Plessis A, Seifert T, Booysen G, Els J. Microfocus X-ray computed tomography (CT) analysis of laser sintered parts. South Afr J Indus Eng 2014;25:39–49.
16. du Plessis A, le Roux SG, Steyn F. X-ray computed tomography of consumer-grade 3D-printed parts. 3D Print Additive Manuf 2015;2:190–195.
17. du Plessis A, le Roux SG, Els J, Booysen G, Blaine DC. Application of microCT to the non-destructive testing of an additive manufactured titanium component. Case Stud Nondestr Test Eval 2015;4:1–7.
18. Reinhart C, Poliwoda C, Guenther T. How industrial computer tomography accelerates product development in light metal casting and injection moulding industry. In: 10th European Conference on Non-destructive Testing 1:19. Available at http://ndt.net/article/ecndt2010/reports/1_09_19.pdf (accessed February 27 2016).
19. Becker B, Maier D, Reinhart C. Computer tomography has arrived in automated inspection processes, combining material and geometry analyses. In: 18th World Conference on Non-Destructive Testing, April 16–20, 2012, Durban, South Africa.

Address correspondence to:
Anton du Plessis
CT Scanner Facility
Central Analytical Facilities
Stellenbosch University
PO Sauer
Stellenbosch 7602
South Africa

E-mail: anton2@sun.ac.za